

4D IMAGE WARPING FOR MEASUREMENT OF LONGITUDINAL BRAIN CHANGES

Dinggang Shen

Section of Biomedical Image Analysis
Department of Radiology, University of Pennsylvania, Philadelphia, PA
Email: *dgshen@rad.upenn.edu*

ABSTRACT

This paper presents a method for robustly measuring temporal morphological brain changes, by means of a 4D image warping mechanism. Longitudinal stability is achieved by considering all temporal MR images of an individual simultaneously in image warping, rather than by individually warping a 3D template to an individual, or by warping the images of one time-point to those of another time-point. Moreover, image features that are consistently recognized in all time-points guide the warping procedure, whereas spurious features that appear inconsistently at different time-points are eliminated. This deformation strategy significantly improves robustness in detecting anatomical correspondences, thereby producing smooth and accurate estimations of longitudinal changes. The experimental results show the significant improvement of 4D warping method over our previous 3D warping method in measuring subtle longitudinal changes of brain structures.

1. INTRODUCTION

Measuring longitudinal changes in brain structure requires highly accurate segmentation and volumetric measurement of brain structures, either manually or by warping of labeled atlas [1]. Manual segmentation requires extensive human interaction and considerable training. Most importantly, both intra-rater reproducibility and inter-rater agreement are difficult to achieve in a longitudinal study, particularly when subtle changes are to be measured. Accordingly, many automatic image segmentation and parcellation methods have been developed [2-12]. We previously proposed a fully automated atlas matching approach, referred to as Hierarchical Attribute Matching Mechanism for Elastic Registration (HAMMER) [13,14]. This approach attempted to overcome limitations of several existing image warping methods.

Regardless of their relative merits and limitations, all of the existing atlas warping techniques were mainly designed for 3D images. Consequently, applying these 3D methods independently for each time-point in a longitudinal study typically leads to noisy longitudinal measurements, particularly for small structures such as the hippocampus, due to inconsistent atlas matching among different time-points. Although one can obtain a smooth estimation of longitudinal changes by smoothing the measurements along the temporal dimension, the smoothed measurements generally deviate significantly from the actual image data, unless smoothing is performed concurrently with atlas warping procedure and by taking into account the image features. Freeborough and Fox *et.al.* [19] attempted to impose

temporal smoothing, by warping the images of one time-point to those of another time-point. However, that approach, too, does not avoid jitter noise between any two differential measurements, since spatial normalization is based on independent warpings between pairs of images.

In this paper, we present an approach that overcomes the above-mentioned limitations. Specially, we propose a fully automatic 4-dimensional atlas matching method that constrains the smoothness in both spatial and temporal domains during the hierarchical atlas matching procedure, thereby producing smooth and accurate estimations of longitudinal changes. Importantly, morphological features guiding this deformation process are determined via 4D image analysis, which significantly reduces noise and improves robustness in detecting anatomical correspondence. Put simply, image features that are consistently recognized in all time-points guide the warping procedure, whereas spurious features, such as noisy edges that appear inconsistently at different time-points, are eliminated.

2. METHOD

2.1. Overview

The proposed approach, referred to as 4D-HAMMER, involves the following two steps:

- (1) Rigid alignment of 3D images of a given subject acquired at different time points, in order to produce a 4D image. We employ 3D-HAMMER to establish the correspondences between neighboring 3D images, and then align one image (time t) to its previous-time image ($t-1$) by a rigid transformation calculated from the established correspondences [15].
- (2) Hierarchical deformation of the 4D atlas to the 4D subject images, via a hierarchical attribute-based matching method. Initially, the deformation of the atlas is influenced primarily by voxels with distinctive attribute vectors, thereby minimizing the chances of poor matches and also reducing computational burden. As the deformation proceeds, voxels with less distinctive attribute vectors gradually gain influence over the deformation.

2.2. Notation

The 4D images studied in this paper have three spatial dimensions (\mathbf{x}) and one temporal dimension (t), where \mathbf{x} and t are the spatial and the temporal coordinates, respectively. Let $T(\mathbf{x}, t)$ denote the intensity of the 4D template image at a point (\mathbf{x}, t) ; therefore, $T_t(\mathbf{x})$ is a usual 3D template image at time t . Similarly, $S(\mathbf{x}, t)$

denotes the intensity of the 4D subject image, and $S_t(\mathbf{x})$ is a usual 3D subject image at time t . The spatial domains for the template and the subject are not necessarily the same; hence, V_T is used for the template's spatial domain and V_S for the subject's spatial domain. However, the temporal domains are assumed to be same, i.e., totally N volumetric images constitute the template and the subject, where $t \in [1, N]$.

Displacement along the temporal dimension is not allowed during the deformable registration procedure, since the 3D images are acquired at known time-points and temporal correspondence is thus known. In this way, the template image $T_t(\mathbf{x})$ is only permitted to warp towards the subject image of the same time t , $S_t(\mathbf{x})$. Accordingly, the displacement field $u(\mathbf{x}, t)$ defines the relative *spatial* deformation of the template image $T(\mathbf{x}, t)$ to the subject image $S(\mathbf{x} + u(\mathbf{x}, t), t)$. Let $h(\mathbf{x}, t)$ be the transformation corresponding to the displacement field $u(\mathbf{x}, t)$: $h(\mathbf{x}, t) = (\mathbf{x} + u(\mathbf{x}, t), t)$. The inverse transformation is $h^{-1}(\mathbf{x}, t)$, which is also known as backward transformation.

2.3. Attribute vector

Each voxel carries its own morphological signature, i.e., an attribute vector $\mathbf{a}(\mathbf{x}, t)$, which is designed to be as distinctive as possible of its respective voxel, in order to facilitate automated matching. Each attribute vector includes edge types, image intensity, and Geometric Moment Invariants (GMIs) at different scales [21], all of which are computed from the 3D spatial images [13]. GMIs at a particular scale are calculated by placing a spherical neighborhood around each voxel, and then calculating a number of parameters that are invariant to rotation [21]. Even richer geometric features, such as those based on Wavelet coefficients, can also be used as image attributes, as we described in [18]. The reason for developing an attribute vector is that, if rich enough, the attribute vector can distinguish between different parts of the image. The detailed definitions for the attribute vectors and the similarity definitions of those vectors can be found in our previous paper [13].

2.4. Mathematical optimization

The 4D-HAMMER algorithm hierarchically optimizes the cost function, E , of attribute vector similarity, which is given below:

$$E = E_F + E_B + E_S, \quad (1)$$

where

$$E_F = \sum_{t=1}^N \sum_{\mathbf{x} \in V_T} \omega_T(\mathbf{x}, t) \left(\frac{\sum_{(\mathbf{z}, \tau) \in n(\mathbf{x}, t)} \varepsilon_T(\mathbf{z}, \tau) (1 - m(\mathbf{a}_T(\mathbf{z}, \tau), \mathbf{a}_S(h(\mathbf{z}, \tau))))}{\sum_{(\mathbf{z}, \tau) \in n(\mathbf{x}, t)} \varepsilon_T(\mathbf{z}, \tau)} \right),$$

$$E_B = \sum_{t=1}^N \sum_{\mathbf{x} \in V_S} \omega_S(\mathbf{x}, t) \left(\frac{\sum_{(\mathbf{z}, \tau) \in n(\mathbf{x}, t)} \varepsilon_S(\mathbf{z}, \tau) (1 - m(\mathbf{a}_T(h^{-1}(\mathbf{z}, \tau)), \mathbf{a}_S(\mathbf{z}, \tau)))}{\sum_{(\mathbf{z}, \tau) \in n(\mathbf{x}, t)} \varepsilon_S(\mathbf{z}, \tau)} \right),$$

$$E_S = \alpha \cdot E_S^{\text{Spatial}} + \beta \cdot E_S^{\text{Temporal}},$$

$$E_S^{\text{Spatial}} = \sum_{t=1}^N \sum_{\mathbf{x} \in V_T} \left\| u(\mathbf{x}, t) - \frac{\sum_{\mathbf{z} \in n(\mathbf{x})} g_1(\|\mathbf{z} - \mathbf{x}\|) u(\mathbf{z}, t)}{\sum_{\mathbf{z} \in n(\mathbf{x})} g_1(\|\mathbf{z} - \mathbf{x}\|)} \right\|^2,$$

$$E_S^{\text{Temporal}} = \sum_{\mathbf{x} \in V_T} \sum_{t=1}^N \left\| u(\mathbf{x}, t) - \frac{\sum_{\tau \in n(t)} g_2(\tau - t) u(\mathbf{x}, \tau)}{\sum_{\tau \in n(t)} g_2(\tau - t)} \right\|^2.$$

The first term E_F measures the similarity of attribute vectors in the vicinity of a point (\mathbf{x}, t) under consideration, and it is therefore guiding the identification of anatomical correspondence, to the extent that anatomical correspondence is reflected by similarity of the voxel-wise signatures. E_F is based on the forward transformation $h(\cdot)$ from the template to the subject. In particular, for each template point (\mathbf{x}, t) , we integrate the attribute vector differences in its 4D (spatio-temporal) neighborhood, denoted by $n(\mathbf{x}, t)$. (\mathbf{z}, τ) is a neighboring point. Thus, $\mathbf{a}_T(\mathbf{z}, \tau)$ is the attribute vector of the template point (\mathbf{z}, τ) , and $\mathbf{a}_S(h(\mathbf{z}, \tau))$ is the attribute vector of the corresponding subject point $h(\mathbf{z}, \tau)$. $m(\cdot, \cdot)$ is the similarity of two attribute vectors, and ranges from 0 to 1. Thus, $(1 - m(\cdot, \cdot))$ is the difference of two attribute vectors. $\varepsilon_T(\mathbf{z}, \tau)$ is the weighting parameter for the points in the neighborhood; large weights are used for the salient points, such as boundary points. $\omega_T(\mathbf{x}, t)$ denotes the importance of the template point (\mathbf{x}, t) in image matching. Large weights are also assigned to the points with distinctive attribute vectors. This assignment allows our algorithm to focus initially only on the distinctive points. By hierarchically assigning weights to the template points, our approach is able to hierarchically deform the images. Moreover, the size of neighborhood $n(\mathbf{x}, t)$ is large initially and decreases gradually with the progress of the deformation, which increases the robustness and accuracy of our algorithm.

The second term E_B is similar to the first one, but it is defined on the inverse transformation $h^{-1}(\cdot)$ from the subject to the template. This term is used to constrain the inverse consistency of the transformation $h(\cdot)$ [16]. Specifically, these first two terms together favor transformations that yield mutually compatible results when deforming the template to the subject and as well as the converse.

The third term E_S is a smoothness constraint for the displacement field, defined on the template space V_T . The displacement field $u(\mathbf{x}, t)$ is penalized if it differs significantly from its average displacement field in the 4D neighborhood. For convenience, we separate this smoothness requirement into two components: a spatial smoothing component, E_S^{Spatial} , and a temporal smoothing component, E_S^{Temporal} . α and β are two weighting parameters. In the spatial smoothing component, we use a Gaussian filter g_1 to obtain the average displacement in a 3D spatial neighborhood $n(\mathbf{x})$. The standard deviation in Gaussian filter g_1 changes adaptively as the deformation proceeds. In the temporal smoothing component, we use another Gaussian filter g_2 to obtain the average displacement in a 1D temporal neighborhood $n(t)$. Selecting different sizes of temporal neighborhood and standard deviation for g_2 will lead to a different degree of smoothness on the displacement fields along the temporal dimension.

2.5. Attribute-based deformable matching strategies

Hierarchical selection of active points. The 4D template is warped to the subject by attempting to match the attribute vectors of a number of points, which we call active points. These are the points with relatively distinctive attribute vectors, which can be identified relatively more reliably based on their morphological signatures. The selection of the active points can be determined purely from their attribute vector values in a training set of images.

This strategy is aimed at speeding up performance and reducing local minima. In the deformable matching procedure, we first evaluate candidate matches of points with distinctive attribute vectors, and then gradually consider points with less distinctive attribute vectors. Effectively, this procedure approximates what would be a very high-dimensional cost function in equation (1), by a significantly lower dimensional function of only the active points. This latter function has few local minima, because it is a function of the coordinates of points for which relatively unambiguous matches can be found.

Hierarchical subvolume deformation strategy. In order to increase robustness to potentially false matches of active points, we evaluate the similarity of attribute vectors in the entire subvolume around an active point, not simply the similarity of active points. In particular, for each template active point, we search for several target points with similar attribute vectors in its neighborhood. For each candidate match, the similarity of attribute vectors in the respective 4D subvolumes is evaluated. This is an important aspect of our method. Say, for example, that a false match within an active point's neighborhood happens to have similar attribute vector. It is unlikely that all points in the spatial as well as temporal neighborhood also have matching attribute vectors, unless this is a true match. The point in the subject 4D image that presents the highest subvolume-derived attribute vector similarity, is finally defined as a correspondence, provided that the similarity is above a pre-specified threshold. This prevents active points that do not find good matches from actively deforming the volume, as would be the case of a single sulcus in the template deforming to a double sulcus in the subject brain. These multiple levels of evaluation of goodness of correspondence add robustness that is necessary in view of the complexity of the human brain anatomy.

On the other hand, correspondences in the reverse direction, i.e., from the subject to the template, are also examined. If these correspondences turn out to be inconsistent with the forward process described above, then a compromise is reached so that inverse consistency is satisfied.

Inverse consistent transformation. An important characteristic of this matching process is that it is inverse-consistent. A transformation is inverse consistent if it finds consistent results when matching a template to a subject versus when it matches a subject to a template [16,13]. However, most automated image warping algorithms are not inverse consistent. An approach to enforcing inverse consistency in a warping process was described in [16]. However, that approach is computationally very demanding. In our approach, we enforce inverse consistency only on the active points, since the warping transformation elsewhere is determined via interpolation from the active points. The

detailed method for obtaining inverse consistent matches on the active points was described in our previous paper [13].

3. RESULTS

4D-HAMMER was used to estimate the longitudinal changes of hippocampal volumes in the MR images of 9 elderly subjects aged 59-78, selected from our ongoing studies in the Baltimore Longitudinal Study of Aging (BLSA) [17]. Annual MR images are available for each subject, while the images of the first 5 years are analyzed in this paper.

We have labeled hippocampal regions in the model by manual definition of a single template brain [20]. By warping the model to the subject, we can warp the mask of the model hippocampi to each subject, thereby resulting in the segmentation of hippocampi from each subject. The performances of 4D- and 3D- HAMMER are compared, which reveals that 4D-HAMMER performs much better than 3D-HAMMER in measuring subtle longitudinal changes of the hippocampus.

Fig 1 shows the hippocampal volumes of a typical subject, detected by 4D- and 3D- HAMMER, respectively. It can be observed that the results by 4D-HAMMER are much smoother than those by 3D-HAMMER. Fig 2 further shows the average hippocampal volumes of 9 subjects estimated by 3D- and 4D-HAMMER, respectively. It can be seen that 3D-HAMMER resulted in noisy longitudinal estimations, while 4D-HAMMER produced smooth longitudinal estimations. Importantly, the percentage of hippocampal shrinkage detected during the 4 years (from year 1 to 5) is only 2.1% by 3D-HAMMER, compared to 5.5% by 4D-HAMMER, and 5.7% by manual delineation of an experienced rater [20]. Notably, the shrinking percentage estimated by 4D-HAMMER is very close to that achieved by an experienced rater.

4. CONCLUSION

We have developed a robust and accurate 4D atlas matching method for registration and warping of 4D images, and for estimating the longitudinal morphological changes of brain structures. The experimental results show that 4D-HAMMER can provide smooth and accurate longitudinal estimations even for small structures such as hippocampus. The main characteristics of our approach are summarized next. *First*, an attribute vector is defined as a morphological signature for every point in a 4D image. The attribute vector is developed to be as distinctive as possible, thereby reducing the ambiguity in correspondence matching and finally avoiding local minima. *Second*, according to the distinctiveness of the attribute vectors, the points in the 4D space are successively selected as active points for hierarchically deforming the template to the subject. This helps us avoid local minima and also speed up the algorithm. *Third*, our approach is further made robust to local minima and noise, by using a 4D subvolume matching and deformation strategy. *Finally*, the displacement fields are preserved to be smooth at both spatial and temporal domains, via appropriate constraints defined in both domains.

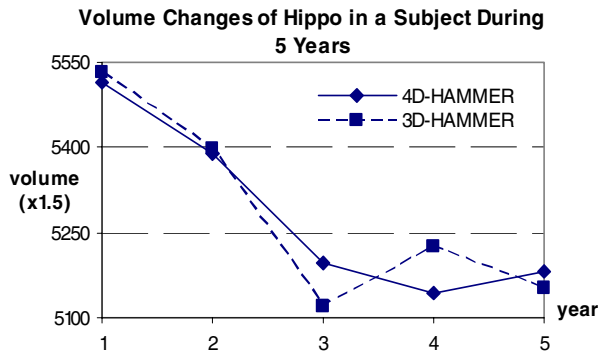


Fig. 1. Comparing the performances of 4D- and 3D- HAMMER in estimating the longitudinal changes of hippocampi from a subject.

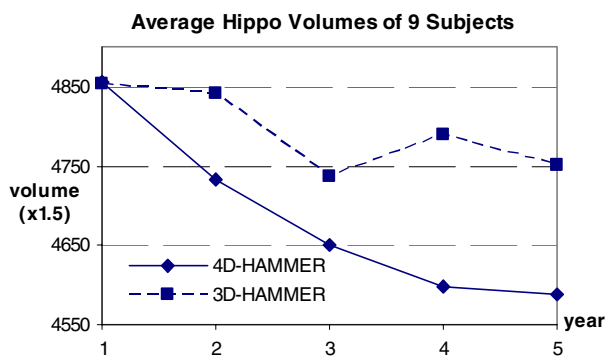


Fig. 2. Average hippocampal volumes of the 9 subjects, estimated by 4D- and 3D- HAMMER, respectively.

REFERENCES

1. M.K. Chung, K.J. Worsley, T. Paus, C. Cherif, D.L. Collins, J.N. Giedd, J.L. Rapoport and A.C. Evans. "A Unified Statistical Approach to Deformation-Based Morphometry", *NeuroImage*, 14(3):595-606, September 2001.
2. M.I. Miller, G.E. Christensen, Y. Amit, U. Grenander. "Mathematical textbook of deformable neuroanatomies". *Proc Nat Acad Sci USA*, 90:11944-11948, 1993.
3. F.L. Bookstein. "Principal Warps: Thin-Plate Splines and the Decomposition of Deformations". *IEEE Trans. on Pattern Analysis and Machine Intelligence*, 11(6):567-585, 1989.
4. K. Rohr. "Image registration based on thin plate splines and local estimates of anisotropic landmark localization uncertainties". *Lect. Notes in Comp. Sci.: MICCAI'98*, Volume 1496, p.1174-1183, 1999.
5. J.P. Thirion, O. Monga, S. Benayoun, A. Guezic and N. Ayache. "Automatic registration of 3-D images using surface curvature". *SPIE Proc., Mathematical Methods in Medical Imaging*, volume 1768, p.206-216, 1992.
6. S.C. Joshi, M.I. Miller, G.E. Christensen, A. Banerjee, T. Coogan and U. Grenander. "Hierarchical brain mapping via a generalized Dirichlet solution for mapping brain manifolds". *Proc. of the SPIE Conf. on Geom. Methods in Applied Imaging*, volume 2573, p.278-289, July 1995.
7. H. Chui, L. Win, R. Schultz, J. Duncan, and A. Rangarajan. "A Unified Feature Registration Method for Brain Mapping".

Information Processing in Medical Imaging, p.300-314, Davis, CA, USA, June 18-22, 2001.

8. P. Thompson and A.W. Toga. "A surface-based technique for warping three-dimensional images of the brain". *IEEE Trans. on Med. Imaging*, volume 15, p.402-417, 1996.
9. M. Breijl and M. Sonka. "Object localization and border detection criteria design in edge-based image segmentation: automated learning from examples". *IEEE Trans. on Med. Imaging*, volume 19, p.973-985, 2000.
10. A.C. Evans, W. Dai, L. Collins, P. Neeling and S. Marett. "Warping of a computerized 3-D atlas to match brain image volumes for quantitative neuroanatomical and functional analysis". *SPIE Proc., Image Processing*, volume 1445, p.236-246, 1991.
11. J.C. Gee, C. Barillot, L.L. Briquer, D.R. Haynor and R. Bajcsy. "Matching structural images of the human brain using statistical and geometrical image features". *Proc. SPIE Visualization in Biomedical Computing*, vol. 2359, pp.191-204, 1994.
12. K.J. Friston, A.P. Holmes, K.J. Worsley, J.P. Poline, C.D. Frith and R.S.J. Frackowiak. "Statistical parametric maps in functional imaging: a general linear approach". *Human Brain Mapping*, pp. 189-210, 1995.
13. D. Shen, C. Davatzikos. "HAMMER: Hierarchical Attribute Matching Mechanism for Elastic Registration". *IEEE Trans. on Medical Imaging*, 21(11):1421-1439, Nov 2002.
14. D. Shen, C. Davatzikos. "Very High Resolution Morphometry Using Mass-Preserving Deformations and HAMMER Elastic Registration". *NeuroImage*, 18(1): 28-41, Jan 2003.
15. S. Umeyama. "Least-squares estimation of transformation parameters between two point patterns". *IEEE Trans. on PAMI*, 13(4):376-380, 1991.
16. G.E. Christensen. "Consistent Linear-Elastic Transformations for Image Matching". *Information Processing in Medical Imaging*, LCNS 1613, Springer-Verlag, pp. 224-237, 1999.
17. S.M. Resnick, A.F. Goldszal, C. Davatzikos, S. Golski, M.A. Kraut, E.J. Metter, R.N. Bryan, and A.B. Zonderman. "One-year age changes in MRI brain volumes in older adults", *Cerebral Cortex*, 10:464-472, 2000.
18. Z. Xue, D. Shen, C. Davatzikos, "Determining correspondence in 3D MR brain images using attribute vectors as morphological signatures of voxels", revised for *IEEE Trans. on Medical Imaging*.
19. P.A. Freeborough, N.C. Fox, "Modeling Brain Deformations in Alzheimer's Disease by Fluid Registration of Serial 3D MR Images". *Journal of Computer Assisted Tomography*, 22: 838-843, 1998.
20. D. Shen, S. Moffat, S.M. Resnick, and C. Davatzikos, "Measuring Size and Shape of the Hippocampus in MR Images Using a Deformable Shape Model", *NeuroImage*, 15(2):422-434, Feb 2002.
21. C.H. Lo, H.S. Don. "3-D Moment Forms: Their Construction and Application to Object Identification and Positioning". *IEEE Trans. on Pattern Analysis and Machine Intelligence*, 11(10): 1053-1064, Oct. 1989.